Temperature-dependent orientational ordering on a spherical surface modeled with a lattice spin model

Alan M. Luo,[1] Stefan Wenk,[1] and Patrick Ilg[1,2]
[1]*ETH Zürich, Department of Materials, Polymer Physics, CH-8093 Zürich, Switzerland*
[2]*School of Mathematical and Physical Sciences, University of Reading, Reading RG6 6AX, United Kingdom*
(Received 9 April 2014; revised manuscript received 30 June 2014; published 18 August 2014)

We study the orientational ordering on the surface of a sphere using Monte Carlo and Brownian dynamics simulations of rods interacting with an anisotropic potential. We restrict the orientations to the local tangent plane of the spherical surface and fix the position of each rod to be at a discrete point on the spherical surface. On the surface of a sphere, orientational ordering cannot be perfectly nematic due to the inevitable presence of defects. We find that the ground state of four $+1/2$ point defects is stable across a broad range of temperatures. We investigate the transition from disordered to ordered phase by decreasing the temperature and find a very smooth transition. We use fluctuations of the local directors to estimate the Frank elastic constant on the surface of a sphere and compare it to the planar case. We observe subdiffusive behavior in the mean square displacement of the defect cores and estimate their diffusion constants.

DOI: 10.1103/PhysRevE.90.022502 PACS number(s): 61.30.Gd, 61.30.Dk, 61.30.Jf

I. INTRODUCTION

Nematic liquid crystals are classical examples of soft matter systems exhibiting broken symmetries [1]. The question how nematic order forms in confined geometries and on curved surfaces is not only of fundamental interest but also relevant for applications [2–4]. For the special case of spherical surfaces, the Poincaré theorem (colloquially known as the "hairy ball" theorem) excludes perfect nematic order. Lubensky and Prost predicted that four point defects of strength $+1/2$ arranged at the vertices of a regular tetrahedron minimize the defect energy [5]. The theoretically expected defect structures are indeed observed in experiments [6] and simulations [7]. Besides the tetrahedral arrangement, other defect structures have been observed experimentally [6,8,9] and in simulations [10], which have been attributed to the finite thickness of the nematic shells [11] or to vastly different values of the splay and bend elastic constants [7].

Starting with the work of Lubensky and Prost [5], the theoretical and simulation studies have so far mostly concentrated on the low-temperature regime and identified the defect structures of the ground or low-energy states. Here we focus on the temperature dependence of various physical quantities that have so far received relatively little attention. In particular, we investigate the growing local and global orientational ordering upon lowering the temperature as well as the elastic and dynamic properties.

In order to study these quantities, we employ Monte Carlo and Brownian dynamics computer simulations to study our model, which is an adapted Lebwohl-Lasher model [12,13] confined to a spherical surface. The original Lebwohl-Lasher model can be considered as the simplest non-mean-field model for the isotropic-to-nematic (IN) transition for bulk liquid crystals, where rigid rotators are arranged on a regular lattice with nearest neighbor interactions. There is some debate in the literature about the nature of this transition in two dimensions, whether it is weakly first order or continuous [14,15]. Here we are interested in the case when the location of the rotators are confined to the surface of a sphere and their orientation vector is confined to the local tangent plane of the sphere, meaning we deal exclusively with a two-dimensional model.

However, since the related case of the planar model (with rotator position and orientation confined to a flat surface) is hardly considered in the literature, we treat this simpler model first. Our results are in agreement with an earlier study that found a continuous transition of planar rotators on a triangular lattice [16]. We note that defects in the planar model were also studied by annealing from a state with random orientations or by using suitable boundary conditions to create topological frustration [17]. On the spherical surface, we find a very smooth increase of local nematic order with decreasing temperature, independent of the particular lattice type employed. We observe that the nematic ordering is characterized by four point defects of strength $+1/2$ in a tetrahedral arrangement not only at very low temperatures but within a broad range in the nematic regime. In addition, we determine the effective elastic constant on the spherical surface and study the thermal diffusive motion of the point defects. The diffusive motion is particularly important given the interest in using functionalized defects in thin nematic shells as directional bonds to mimic atomic bonding [4].

The paper is organized into two main sections, the first, Sec. II deals with the planar model when the rod positions and spins are confined to a plane. We investigate orientational ordering and the elastic constant of this system. We introduce the spherical model and our simulation technique in Sec. III. We further discuss in the subsections orientational ordering on a sphere, defect mobility, and the behavior of the Frank elastic constant. Concluding remarks are made in Sec. IV.

II. PLANAR MODEL

We consider a simple lattice model of a nematic system, where rigid rotators ("spins") $\mathbf{u}_j$ are arranged on a regular lattice. Nearest neighbor attractions favor parallel spin orientation, described by the Hamiltonian

$$H = -\frac{\varepsilon}{2}\sum_{\langle i,j\rangle} T_2(\mathbf{u}_i \cdot \mathbf{u}_j), \tag{1}$$

where the sum runs over the nearest neighbor pairs i and j on a given lattice and ε is the interaction strength between spins (or can be interpreted as the energy of a bond between two spins). The factor of $1/2$ avoids double counting the bond energies. We choose $T_2(x) = 2x^2 - 1$ as the second Chebyshev polynomial so that the energy of the isotropic state is zero [18]. The orientations of the spins are normalized $\mathbf{u}_j^2 = 1$.

We note that in most previous studies of the so-called planar Lebwohl-Lasher model, the spins $\mathbf{u}_j$ are arranged on a two-dimensional planar lattice and are allowed to rotate in three dimensions, and $T_2(x)$ is instead chosen as the second Legendre polynomial $P_2(x) = (3x^2 - 1)/2$ [14,15]. This particular model displays a continuous transition from an isotropic phase at high temperatures to a nematic state below a critical temperature, which according to recent finite-size scaling studies is around $k_B T_c/\varepsilon \approx 0.56$ on a square lattice [15].

A. Orientational ordering and the isotropic-nematic transition

Since no exact solution is known to date for our two-dimensional model, we study the transition theoretically by several approaches: using a mean-field approximation, using the Landau-de Gennes free energy, and using computer simulations. Begin with the mean-field approximation so that the Hamiltonian is simplified to [19]

$$H^{\mathrm{MF}} = -2\varepsilon z Q \sum_i [T_2(\mathbf{u}_i \cdot \mathbf{n}) - Q], \tag{2}$$

where z is the coordination number of the lattice and Q is defined as the greatest eigenvalue of the orientation tensor $\mathbf{Q}$ with corresponding eigenvector $\mathbf{n}$

$$\mathbf{Q} = \frac{1}{N} \sum_i^N \left(\mathbf{u}_i \mathbf{u}_i - \frac{1}{2}\mathbf{1} \right). \tag{3}$$

The eigenvector $\mathbf{n}$ is called the director and it represents the direction of preferred alignment of the spins while Q measures the degree of alignment of the spins; it varies between 0 and $1/2$ for isotropic and perfectly ordered states, respectively. The mean-field free energy implies a self-consistency relation for the order parameter that can be expanded for small Q to give the mean-field prediction for the transition temperature $k_B T_c^{\mathrm{MF}}/\varepsilon = z/2$. Further details are given in Appendix A.

An alternative approach has been recently employed by two of the authors to systematically obtain the macroscopic Landau-de Gennes free energy starting from a microscopic model [20]. The ideal orientational entropy for noninteracting planar rotators was found to be given by $S^{\mathrm{ideal}}(Q) = Nk_B(-4Q^2 - 4Q^4) + \mathcal{O}(Q^6)$ for weak ordering. Following earlier work [21], we obtain the Landau-de Gennes free energy by adding the mean interaction energy $E^{\mathrm{MF}} = \langle H^{\mathrm{MF}} \rangle = -2N\varepsilon z Q^2$ of the Lebwohl-Lasher model, $F^{\mathrm{LG}} = E^{\mathrm{MF}} - TS^{\mathrm{ideal}}$, to obtain

$$F^{\mathrm{LG}}(Q) = Nk_B T[(4 - 2\beta\varepsilon z)Q^2 + 4Q^4] + \mathcal{O}(Q^6). \tag{4}$$

Due to the absence of a cubic invariant, the Landau-de Gennes free energy (4) predicts a continuous transition at the same reduced temperature $k_B T_c^{\mathrm{LG}}/\varepsilon = z/2$ as the mean-field prediction.

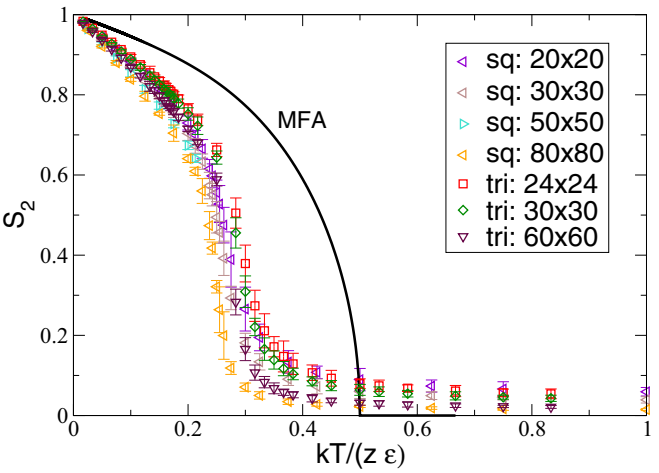

FIG. 1. (Color online) Two-dimensional order parameter S_2 as function of the reduced temperature $k_B T/z\varepsilon$ for our planar model on a square ($z = 4$) and triangular ($z = 6$) grid for different system sizes. The solid black line indicates the mean-field prediction. Our results are in agreement with those shown in Fig. 4 of Ref. [16].

We study the exact model with the help of Monte Carlo (MC) simulations on two-dimensional square ($z = 4$) and triangular ($z = 6$) lattices. We use a standard Metropolis algorithm, where the individual attempt moves are rotations of randomly selected single spins. The maximal rotation was adapted so that, on average, roughly half of the attempted moves are accepted. Different lattice sizes ranging from 20×20 ($N = 400$) up to 80×80 ($N = 6400$) spins are considered in order to estimate finite-size effects. Typically, 2×10^6 MC steps are used for equilibration, followed by another 6×10^6 MC steps for data collection, where one MC step consists of N attempted moves. Statistical errors are estimated from block averages.

Figure 1 shows the results for the two-dimensional order parameter $S_2 = 2Q$ obtained from MC simulations on a square and triangular lattice together with the mean-field prediction. As suggested theoretically, the simulation data approximately collapse onto a master curve when plotted as a function of reduced temperature $k_B T/(z\varepsilon)$. It has already been noted in [16] that the mean-field prediction for the transition temperature $k_B T_c^{\mathrm{MF}}/(z\varepsilon) = 1/2$ is in poor agreement with the numerical results. On a triangular lattice, MC simulations showed a continuous transition at $k_B T_c/\varepsilon = 1.8 \pm 0.1$ [16], corresponding to $k_B T_c/(z\varepsilon) = 0.30 \pm 0.02$, in agreement with our data.

B. Frank elastic constant

We now consider the elastic properties of the planar model. In a two-dimensional nematic phase, there are, in general, two Frank elastic constants K_1, K_3 due to bend and splay distortions of the director field [22]. In the Lebwohl-Lasher model and its two-dimensional variant considered here, the one-constant approximation $K = K_1 \approx K_3$ holds, and the Frank elastic energy in d dimensions is given by [22]

$$F_{\mathrm{el}} = \frac{1}{2} K \int d^d x (\nabla_\alpha n_\beta)(\nabla_\alpha n_\beta). \tag{5}$$

For planar rotators, the director can be expressed as $\mathbf{n} = (\sin\theta, \cos\theta)$ and $F_{\rm el}$ simplifies to $F_{\rm el} = \frac{1}{2}K\int d^2x|\nabla\theta|^2$. From the Fourier representation of the director angle fluctuations,

$$\delta\theta(\mathbf{x}) = \frac{1}{L^2}\sum_{\mathbf{q}}\delta\tilde{\theta}(\mathbf{q})e^{i\mathbf{q}\cdot\mathbf{x}}, \tag{6}$$

we obtain

$$F_{\rm el} = \frac{K}{2L^2}\sum_{\mathbf{q}}\mathbf{q}^2|\delta\tilde{\theta}(\mathbf{q})|^2. \tag{7}$$

Following common practice [23], we employ the equipartition theorem to relate the elastic constant K to the long-wavelength mean-square fluctuations of the director angle

$$\langle|\delta\tilde{\theta}(\mathbf{q})|^2\rangle = \lim_{\mathbf{q}\to 0}\frac{k_{\rm B}TL^2}{K\mathbf{q}^2}. \tag{8}$$

Equation (8) is the analog of the well-known relation for three-dimensional rotators. Adapting a simple argument [24] to the present model gives the theoretical prediction for the planar square lattice $K_{\rm sq} = 4\varepsilon S_2^2$. Details of the calculation are provided in Appendix C.

We determine the left hand side of Eq. (8) from numerical simulations, where we analyze the fluctuations of the orientations relative to the instantaneous director using two-dimensional Fourier transformations. We observe that $\langle|\delta\tilde{\theta}(\mathbf{q})|^2\rangle^{-1}$ indeed scales as $\mathbf{q}^2$ for low $\mathbf{q}$ values as shown in the inset of Fig. 2. From fits of the simulation results to Eq. (8), we obtain the value of the elastic constant K. For low temperatures, the simulation results are in good agreement with the theoretical prediction $K_{\rm sq} = 4\varepsilon S_2^2$, when we use the simulation result for $S_2(T)$. Note, however, that at high temperatures, the slope $1/\langle\tilde{\theta}(\delta\mathbf{q})^2\rangle$ decreases and becomes very small, meaning we could not reliably extract values for the elastic constant beyond $k_{\rm B}T = 0.5$. Figure 2 shows the Frank constant plotted against temperature for a square lattice of size 41×41.

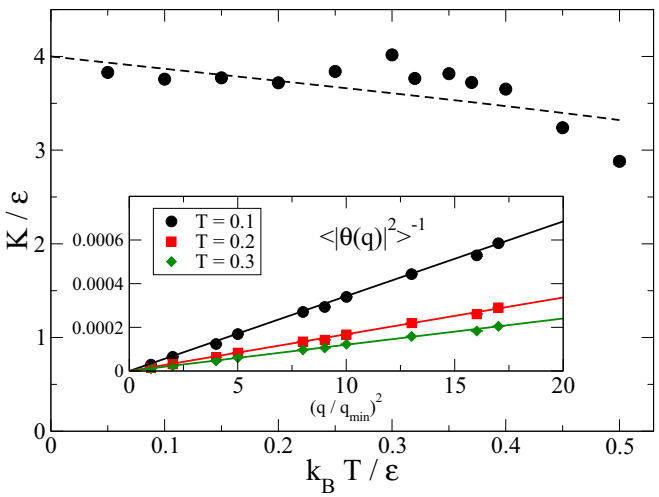

FIG. 2. (Color online) The Frank elastic constant on a square lattice plotted against the reduced temperature. The dashed black line is the theoretical prediction. (Inset) Mean square fluctuation of the director angle plotted against wave number, showing the $1/q^2$ dependence. Symbols are simulation results, whereas lines indicate fits to Eq. (8).

III. SPHERICAL MODEL

Consider now the same system of spins interacting with the same Hamiltonian of Eq. (1) where the lattice is not in the Euclidean plane but covers the surface of a sphere. The spins themselves are constrained to rotate in their local tangent plane. The related model of hard spherocylinders confined to a spherical surface was used in Ref. [7] to discuss experimental results [6].

While the static properties can again be obtained by MC simulations, we here employ Brownian dynamics of the model to study not only the orientational ordering but also the Frank elastic constant and defect dynamics. We present the numerical implementation here, which is an extension of the Brownian dynamics of Ref. [18]. Begin by considering the torque balance on spin i in the overdamped limit

$$\mathbf{T}_i^{\rm fric} + \mathbf{T}_i^{\rm pot} + \mathbf{T}_i^{\rm B} = 0, \tag{9}$$

where $\mathbf{T}_i^{\rm B}$ is the Brownian contribution to the torque and the torques due to rotational friction $\mathbf{T}_i^{\rm fric}$ and interaction potential $\mathbf{T}_i^{\rm pot}$ are defined, respectively, as

$$\mathbf{T}_i^{\rm fric} = -\xi\mathbf{u}_i\times\dot{\mathbf{u}}_i, \tag{10a}$$

$$\mathbf{T}_i^{\rm pot} = \frac{\partial H}{\partial\mathbf{u}_i}\times\mathbf{u}_i, \tag{10b}$$

where ξ is the rotational friction coefficient. The first order Euler-Maruyama integration scheme then reads

$$\Delta\mathbf{u}_i(t) = \Delta\boldsymbol{\omega}_i(t)\times\mathbf{u}_i(t), \tag{11}$$

with

$$\Delta\boldsymbol{\omega}_i(t) = \frac{1}{\xi}\mathbf{T}_i^{\rm pot}(t)\Delta t + \sqrt{2D\Delta t}\,\mathbf{W}_i(t), \tag{12}$$

where $D = k_{\rm B}T/\xi$ is the rotational diffusion coefficient of an isolated spin, $\mathbf{W}_i(t)$ is a three-dimensional Wiener process, and Δt is the time step. For the numerical implementation, we make Eq. (11) dimensionless and write it out explicitly

$$\Delta\mathbf{u}_i(t) = \left[\sum_{j\,(\mathrm{nn}\,i)} 3\,U(\mathbf{u}_i\cdot\mathbf{u}_j)(\mathbf{u}_i\times\mathbf{u}_j)\Delta t_D + \sqrt{2\Delta t_D}\,\mathbf{W}_i(t)\right]\times\mathbf{u}_i, \tag{13}$$

where $U = \varepsilon/k_{\rm B}T$ is the reduced energy, $\Delta t_D = D\Delta t$ is the time step measured in terms of the inverse diffusion coefficient and the sum runs over the nearest neighbors j of spin i (not including spin i). Finally, the new orientation of spin i is obtained by projecting back to the local tangent plane at spin i and normalizing

$$\mathbf{u}_i(t+\Delta t) = \frac{\mathbf{P}_i\cdot[\,\mathbf{u}_i(t)+\Delta\mathbf{u}_i(t)\,]}{|\mathbf{P}_i\cdot[\,\mathbf{u}_i(t)+\Delta\mathbf{u}_i(t)\,]|}, \tag{14}$$

where $\mathbf{P}_i = \mathbf{1} - \mathbf{e}_i\mathbf{e}_i$ is the projector onto the local tangent plane of spin i and $\mathbf{e}_i$ is the normal vector to the spherical surface at spin i. In addition to the global order parameter Q,

we define a *local* order parameter Q_i, given by the greater eigenvalue of the (two-dimensional) orientation tensor,

$$\mathbf{Q}_i = \frac{1}{N_i} \sum_{j\,(\mathrm{nn}\,i)} \left[\frac{(\mathbf{P}_i \cdot \mathbf{u}_j)(\mathbf{P}_i \cdot \mathbf{u}_j)}{|\mathbf{P}_i \cdot \mathbf{u}_j|^2} - \frac{1}{2}\mathbf{1} \right], \qquad (15)$$

Note that for Eq. (15), the neighbors of spin i can be nearest neighbors, or next nearest, etc. We further define the local two-dimensional order parameter as $S_{2i} = 2Q_i$, which varies from zero to one in the isotropic and perfectly ordered phases respectively. We typically used 2–5 $\times$ 10^6 Brownian dynamics steps for equilibration and 4×10^6 steps for collection of averages, with a time step $\Delta t_D = 10^{-3}$; the bare dimensionless rotational diffusion coefficient is $D = 1/2$.

A. Choice of spherical lattice

There are many different methods to construct a regular lattice on the surface of a sphere. Here we want to use a lattice that is as uniform as possible. We therefore try a geodesic grid, Kurihara's grid [25], and a so-called repulsive particle (RP) grid [26] formed by initially randomly distributing the lattice points; one point is fixed and the rest are free to move on the spherical surface. Each lattice point has a repulsive $1/r$ interaction potential and the final grid is formed by minimizing the energy of the system and fixing the remaining lattice points. Each of the lattice points on the three grids has on average six well-defined nearest neighbors. The grids we use all have a mean coordination number of $z = 6 \pm 0.05$. To show that the choice of grid has, at most, a negligible impact on our results we present data for the mean local order parameter $\langle S_{2i} \rangle$ and total energy E plotted against the reduced temperature $k_\mathrm{B}T/\varepsilon$. The mean local order parameter is defined as the mean of S_{2i} over all the N lattice sites. We find the geodesic and RP grids to be indistinguishable within the statistical uncertainty and the Kurihara grid (which has the least isotropically distributed lattice sites) to be very close to the other two.

We see from Fig. 3 that for all the lattices, the system undergoes a smooth transition from nematic to isotropic phase upon increasing the temperature. We also see that the mean local ordering is always lower for the spherical lattice than for the planar case. We further note that both planar and spherical lattices tend to the expected value $E^\mathrm{pot} \to -\varepsilon z N/2$ for perfect nematic ordering. Clearly, the presence of four topological defects on the spherical grids reduces the average orientational order, thereby increasing the potential energy in the nematic phase.

It is worth noting that even at high temperatures, $\langle S_{2i} \rangle$ has a rather large finite value. This is due to a peculiarity of local ordering, where we average over a relatively small sample, e.g., nearest neighbors. This means that even uncorrelated orientations lead to a nonzero local order parameter. This effect decreases as the sample size increases, which is seen in Fig. 3. Furthermore, we calculate the theoretical mean local order parameter in the isotropic state and find that it scales as $\langle S_{2i} \rangle = 1/\sqrt{N_i}$, where N_i is the number of spins over which we average to find S_{2i}; see Appendix B . For nearest neighbors, $N_i = 6$ and we predict $\langle S_{2i} \rangle \approx 0.41$ for the high-temperature disordered regime, which is in agreement with the simulation data shown in Fig. 3. For further studies, particularly regarding finite-size effects on the ordering, we use the RP grid since the number of lattice points on such a grid can be chosen arbitrarily.

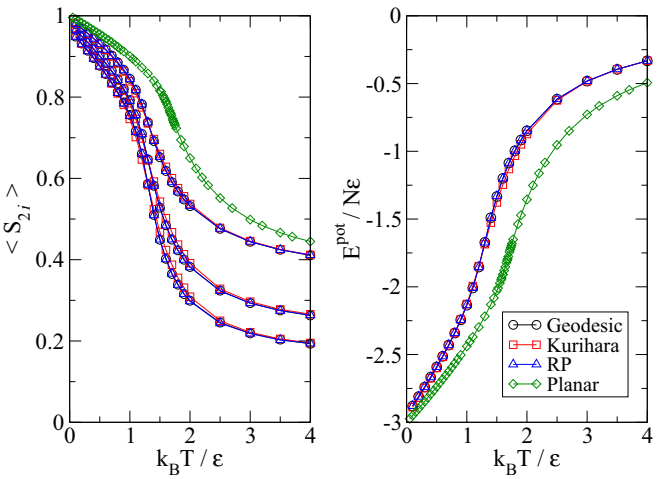

FIG. 3. (Color online) (Left panel) The mean local order parameter $\langle S_{2i} \rangle$ plotted as a function of temperature for the three spherical lattices and triangular planar lattice. For the spherical lattices, the upper (middle, lowest) curve represents taking the sum in Eq. (15) to be over the nearest (next-nearest, next-next-nearest) neighbors, while for the planar grid, the sum is only over nearest neighbors. (Right panel) The total energy per spin plotted as a function of temperature. The planar grid contains $N = 45 \times 45$ points, whereas the spherical grids contain $N \approx 2500$ points. Errors are smaller than the symbol size and lines are guides for the eye.

B. System size effects on orientational ordering

Applications involving larger colloidal liquid crystal formers adsorbed on a closed curved surface like a droplet, so-called colloidosomes, are undoubtedly affected by the finite size of the bubble and the number of attached particles. Therefore, we study the effect of finite size on nematic ordering on the surface of a sphere. We perform Brownian dynamics simulations with the scheme described above using the RP grid with $N = 250, 500, 1000, 2000, 4000, 8000, 16\,000$ for a range of temperatures. Each RP grid has an average coordination number of 6 ± 0.01. The mean local order parameter $\langle S_{2i} \rangle$ plotted against the reduced temperature is shown in Fig. 4, where we see a considerable difference of $\langle S_{2i} \rangle$ between the different grid sizes in the ordered phase below $N = 2000$. Note, however, there is no sharpening of the transition for larger system sizes, as one would expect for critical phenomena.

Ideally, nematic defects on a spherical surface are point defects; however, since we have a finite density of spins and include thermal fluctuations, the local order parameter varies smoothly from its value far from the defect to its minimum within the defect. Therefore, the defects occupy some finite area, which we call the defect core. Since there is no observable finite-size effect on local ordering in the isotropic state, we propose that the defect cores occupy roughly the same number of lattice sites N_c irrespective of the total number of points. For smaller grids, the mean local order parameter is lower because

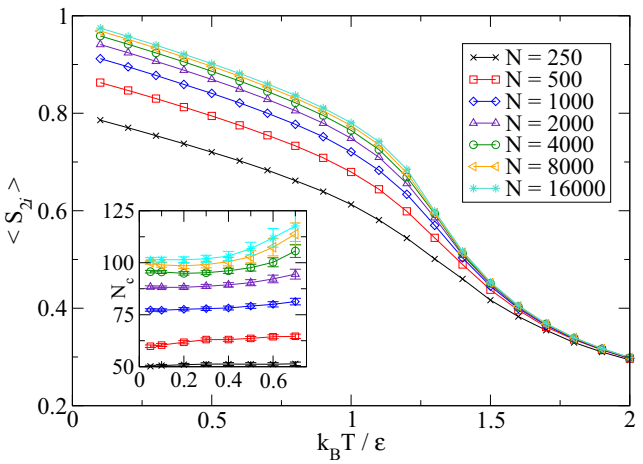

FIG. 4. (Color online) The mean local order parameter $\langle S_{2i}\rangle$ plotted as a function of temperature for various RP grid sizes; see legend. (Inset) Estimate of the number of spins in the defect core N_c plotted against temperature. Errors are smaller than the symbol size unless otherwise shown, and lines are guides for the eye.

the proportion of sites covered by the core N_c/N is greater than for grids with more points.

We estimate the defect core size by finding the center of each defect and counting the number of spins with $S_{2i} < 0.75\langle S_{2i}\rangle$ within solid angles with apex angle $\pi/6$ whose centers coincide with the defect centers. We restrict the counting to be within the aforementioned solid angles to reduce the contribution to our estimate of N_c from thermal fluctuations of S_{2i}. The criteria $S_{2i} < 0.75\langle S_{2i}\rangle$ we use to estimate whether a spin is in the defect core or not is admittedly arbitrary, but this gives more consistent results than other values we have tried.

Our estimate of defect size is shown in the inset of Fig. 4, which indicates that the defect size is roughly constant across the range of temperatures studied; however, we still see a contribution from thermal fluctuations of S_{2i} that occur within the solid angles, especially for the larger systems, which have a greater density of lattice sites and therefore more sites located within the solid angles. Our upper estimate of N_c does increase for larger system sizes, but it scales far more slowly than with N. We also note that our above argument explaining the system size dependency of $\langle S_{2i}\rangle$ leads to the following relationship: $\langle S_{2i}\rangle = 1 - N_c/N$, which should be valid for low temperatures when thermal fluctuations are negligible. As an example, we look at the $N = 250$ case. Here the defect cores contain about 52 lattice sites. From the above formula we would estimate $\langle S_{2i}\rangle \approx 0.79$, which is very close to the observed value. Similarly for the $N = 4000$ case, we predict from the defect core size that for low temperatures $\langle S_{2i}\rangle \approx 0.97$, again, with very good accuracy.

C. Frank elastic constant

An important material parameter is the Frank elastic constant K that measures the free energy cost associated with distortions of the director field [22]. It is a common practice to assume a value of K_s for nematic ordering on a spherical surface to be identical to the corresponding value on a flat plane K. To the best of our knowledge, an independent determination of K_s has not yet been reported. On a spherical surface, the Frank elastic energy takes the form [5]

$$F = \frac{1}{2}K_s \int d^2x\, [\sqrt{g}(D_i n^j)(D^i n_j)], \tag{16}$$

where g is the determinant of the metric tensor, $D_i n^j = \partial_i n^j + \Gamma^j_{ik} n^k$ is the covariant derivative, and Γ^j_{ik} is the Cristoffel symbol. The usual method to obtain an expression relating fluctuations of the director to the Frank elastic constant rely on expressing the Frank free energy in terms of the Fourier modes of the director field and using equipartition to relate the long-wavelength fluctuations of $\mathbf{n}$ to the elastic constant (see Sec. II B and Refs. [27,28]). This method does not work for a spherical surface since Eq. (16) is not diagonalized so plane waves are not independent and equipartition cannot be easily applied.

On the other hand, Refs. [27,28] provide an expression relating the mean square difference of the *local* director angle $\theta(t)$ with elastic constant K,

$$\sigma^2(t) = \langle|\theta(t) - \theta(0)|^2\rangle = \frac{k_B T}{2\pi K}\ln\left(1 + \frac{K}{\nu\alpha}t\right), \tag{17}$$

where ν is the rotational viscosity and α is the area over which the director is measured. Although Eq. (17) was derived for planar geometries, we nevertheless use it to fit our data to obtain K_s for different system sizes and temperatures. Since the Frank elastic energy due to director distortions is only valid in the ordered phase, we limit our investigation to the low-temperature regime.

The time step we use is $\Delta t_D = 10^{-4}$ since we are looking at relatively rapid fluctuations. We use the same number of Brownian dynamics steps for equilibration and averaging as before. The autocorrelation function $\sigma^2(t)$ is calculated using a moving window over the time series of the director angle $\theta(t)$ to obtain better statistics.

Although the derivation of Eq. (17) is technically only valid for a planar system, we find that our data shown in the inset of Fig. 5 has a very good match to the form of Eq. (17). We note that in contrast to Eq. (8), Eq. (17) is a purely local relation that can be applied to the present case. From the fit we extract a value of K_s as a function of temperature for various system sizes, shown in Fig. 5. Despite the uncertainty in fitting parameters, we find that at lower temperatures, the elastic constant K_s is slightly higher for larger system sizes. Similar to the previously noted system size effect in Sec. III B, we expect the finite size of the defect cores to play a greater role in reducing the elastic constant in smaller systems. We plot K_s in terms of the order parameter squared in Fig. 6 in order to compare to the theoretical prediction (see Appendix C) of

$$K_{\text{tri}} = 6\,\varepsilon\, S_2^2. \tag{18}$$

We find that a fit of the form

$$K_s = A\langle S_{2i}\rangle^2 + B, \tag{19}$$

where for our particular data $A = 97$ and B (which depends on system size N) is chosen to yield $K_s = 0$ in the isotropic phase; note again that in our case, isotropic corresponds to a nonzero value of the local order parameter $\langle S_{2i}\rangle$. It is unsurprising that the theoretical estimate is far from correct since in

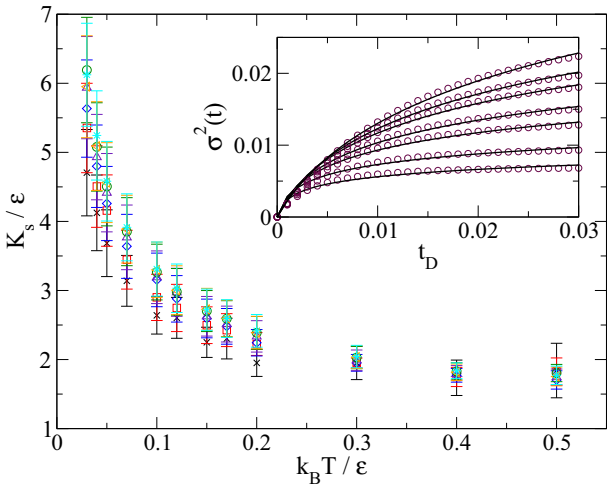

FIG. 5. (Color online) The Frank elastic constant K_s obtained from Eq. (17) plotted against the temperature using the same symbol and color convention as Fig. 4. (Inset) Solid lines are the fit of Eq. (17) to the $N = 4000$ system for $k_B T/\varepsilon = 0.05, 0.07, 0.10, 0.12, 0.15, 0.17, 0.20$.

the derivation (Appendix C) we took the long-wavelength limit to obtain $A = 6$ and this limit is problematic for a spherical surface. On the other hand, there is a clear quadratic dependence on $\langle S_{2i} \rangle$, which is reassuring since this part of the derivation depends only on a mean-field approximation, which does not distinguish between planar or curved surfaces.

The elastic constant K for the 45×45 planar triangular case is also shown in Fig. 6 with its fit to Eq. (19). We find that $K = 6.75\,\varepsilon\,\langle S_{2i} \rangle^2$ yields a good fit, which is not far from the theoretical prediction of Eq. (18). However, it is clear that the planar triangular result differs both qualitatively and quantitatively from the spherical case, and we note that the spherical Frank constant has a noticeable system-size dependency due to the presence of defects.

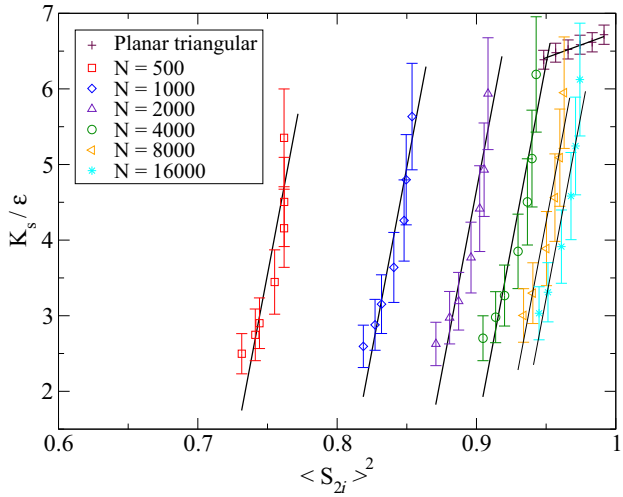

FIG. 6. (Color online) The Frank elastic constant K_s plotted against $\langle S_{2i} \rangle^2$ for different system sizes showing a quadratic dependence. We include the 45×45 planar triangular case. Solid black lines are fits to Eq. (19).

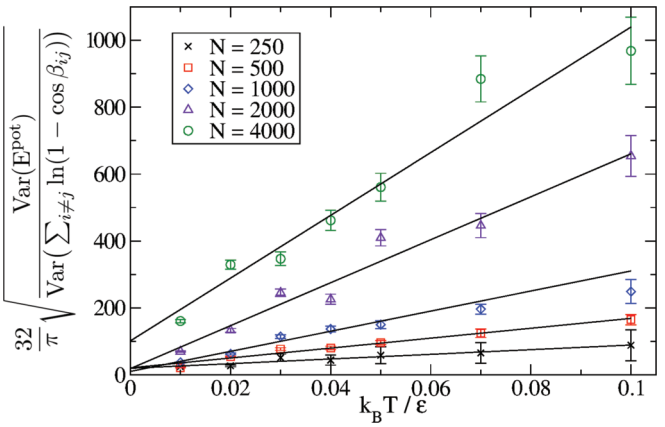

FIG. 7. (Color online) Estimate of the Frank constant using Eq. (20). Solid black lines are linear fits to the data extrapolated back to $T = 0$.

We also attempted to estimate K_s using an alternative method, which makes use of the relationship between defect positions and free energy. The elastic constant is estimated by

$$\mathrm{Var}(E^{\mathrm{pot}}) = \left(\frac{\pi K_s}{32}\right)^2 \mathrm{Var}\left[\sum_{i \neq j} \ln(1 - \cos \beta_{ij})\right], \qquad (20)$$

where $\mathrm{Var}(\cdots)$ denotes the variance of the quantity in brackets, β_{ij} is the angle between defects i and j, and it should be understood that E^{pot} and β_{ij} fluctuate in time. We outline the derivation of Eq. (20) in Appendix D. The main difficulty with this method is that we cannot separate contributions to $\mathrm{Var}(E^{\mathrm{pot}})$ from random thermal fluctuations and from the motion of defects. Therefore, we always overestimate the elastic constant using this method, particularly for higher temperatures, which is shown in Fig. 7. A better way is to estimate K_s by extrapolating $\mathrm{Var}(E^{\mathrm{pot}})$ as $T \to 0$; the values of K_s thus obtained are of the same order of magnitude as the low-temperature portion of Fig. 5. In summary, this method seems to be less accurate and less generally applicable than the alternative method based on director fluctuations. We also tried a third route to determining the Frank elastic constant by using a relationship between the defect core size and the free energy; see Eq. (2) in Ref. [5]. However, since it is difficult to accurately define a defect core size, we found this method yields rather inaccurate estimates.

D. Defect structure and mobility

According to the Poincaré-Hopf theorem, the net topological charge of nematic defects on a spherical surface must be 2. Since the energy of a defect is proportional to the square of its charge and like defects repel each other, Lubensky and Prost predicted that the director field should be composed of four point defects of strength $+1/2$ arranged at the edges of a regular tetrahedron [5]. The theoretical predictions have been confirmed in recent simulations [7] and experiments [6]. Our simulations also reproduce this defect structure and extend earlier simulations [7] to a broad range of temperatures in the nematic regime.

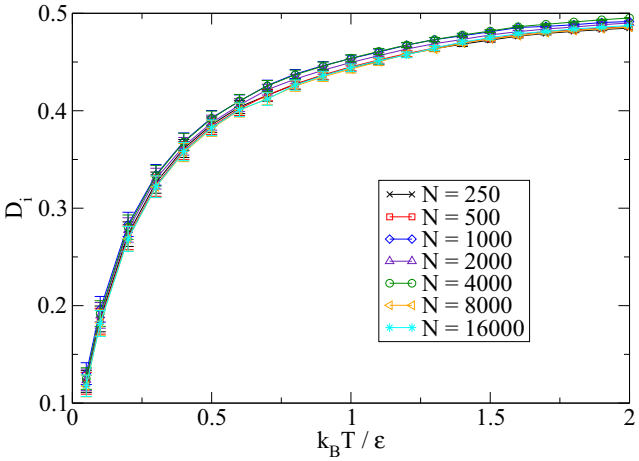

FIG. 8. (Color online) The single particle rotational diffusion constant D_i plotted against temperature. Uncertainties are estimated from the 95% confidence intervals from the fit to Eq. (21).

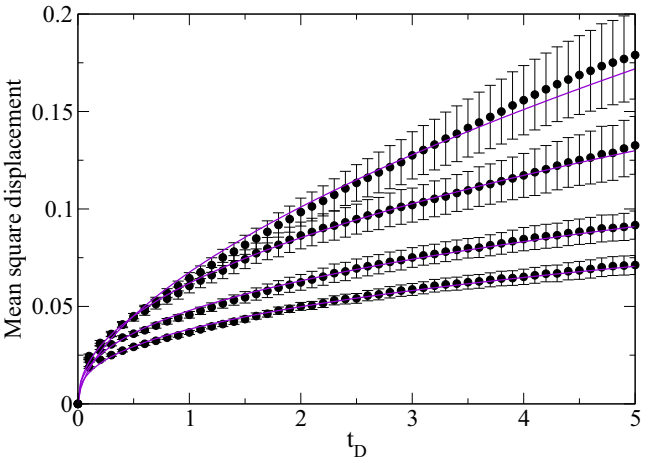

FIG. 10. (Color online) The average mean square displacement of the four defects for the $N = 250$ system for various temperatures. From the top $T = 0.30, 0.20, 0.10, 0.05$. Solid lines are fits to Eq. (23).

There has been recent interest in making use of functionalized defects in thin nematic shells on spherical colloidal particles to serve as directional bonds [4]. With a tetrahedral arrangement of defects, one can mimic sp^3 hybridized atoms such as carbon. It is therefore of great interest to study the motion of defects on spherical surfaces.

We begin by examining the single particle rotational diffusion constant D_i, obtained from

$$C_i(t) = \langle \mathbf{u}_i(t) \cdot \mathbf{u}_i(0) \rangle \sim \exp(-2D_i t). \tag{21}$$

This is expected to be below the bare rotational diffusion constant D, due to the interactions, which hinder rotation. We see in Fig. 8 that this is indeed the case, and that $D = 1/2$ serves as an asymptotic high-temperature (noninteracting) limit.

From visualizations of the Brownian dynamics simulations, it is clear that the defects are not stationary but moving; see Fig. 9. We also show in Fig. 9 agreement with theoretical predictions [5]; we find four point defects of strength $+1/2$ on our sphere arranged on the vertices of a tetrahedron. In order to characterize their motion, we first define the defect

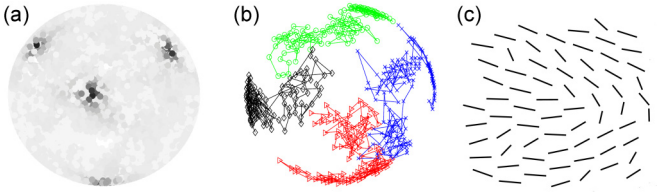

FIG. 9. (Color online) Snapshots of the $N = 4000$, $k_B T/\varepsilon = 0.20$ system showing the following. (a) The local order parameter S_{2i}; darker circles indicate lattice sites with a lower value of S_{2i}. There is some transparency to allow all four defects to be seen in a tetrahedral arrangement. (b) Position of each defect every 10^4 Brownian dynamics steps after a long time: 2×10^6 total steps with $\Delta t_D = 10^{-3}$. Each defect is denoted by black diamonds, green circles, red triangles, and blue crosses, respectively. (c) The orientation of spins in the vicinity of a defect consistent with a topological charge of $+1/2$.

locations $\mathbf{R} = R\,\hat{\mathbf{r}}$ with radial unit vector $\hat{\mathbf{r}}$ and $R = 1$ the radius of the unit sphere. The defect locations are defined as the positions where the local nematic order parameter obtained from next-next-nearest neighbors attains a local minimum. Averaging the local order parameter over next-next-nearest neighbors has the effect of smoothing out thermal fluctuations, allowing easier determination of the defect positions. We do not restrict the defect position to be on a lattice site; rather we take the values of S_{2i} at the discrete lattice points and use bicubic interpolation over a very finely spaced mesh in the vicinity of a defect to locate its exact position. The mean square defect displacement on the spherical surface is calculated using

$$\langle (\Delta\sigma)^2 \rangle = \langle \{ R \cos^{-1}[\hat{\mathbf{r}}(t) \cdot \hat{\mathbf{r}}(0)] \}^2 \rangle, \tag{22}$$

so that the defect diffusion constant D_d is obtained by fitting to Eq. (22),

$$\langle (\Delta\sigma)^2 \rangle = 2d\,D_\mathrm{d}\,t^\alpha, \tag{23}$$

where d is the dimensionality of the system (in our case $d = 2$) and α is a parameter that characterizes motion as subdiffusive ($\alpha < 1$), diffusive ($\alpha = 1$), or superdiffusive ($\alpha > 1$). Again, we use a moving window over the time series of defect position to obtain better statistics. Note that the size of the moving window is limited to the time taken for a defect to diffuse a distance $\pi/6$ in order to avoid periodicity effects due to the spherical geometry.

We find that the defect motion for short times is subdiffusive, with $\alpha < 1$. Fits to Eq. (23) for a selection of temperatures for the $N = 250$ system are shown in Fig. 10. The index α is found to depend on temperature; for higher temperatures the defects become more and more diffusive, see Fig. 11.

The diffusion constants D_d extracted from these fits are shown in Fig. 12. These increase with temperature in a roughly linear fashion. There are also clear system size effects, with the larger system sizes possessing a smaller diffusion constant. In order to maintain the energetically favorable tetrahedral arrangement of defects, it is necessary for the defects to move in a correlated fashion. Furthermore, these defects are not true "Brownian" particles; rather they move through a collective

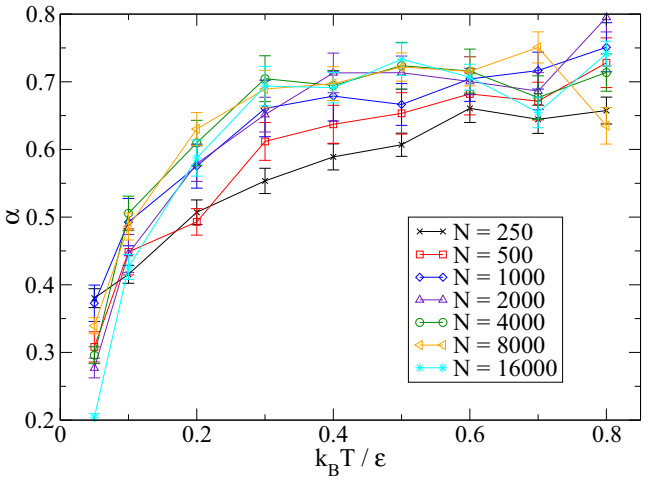

FIG. 11. (Color online) The index α characterizing diffusive behavior as a function of temperature for different system sizes.

rearrangement of spin orientations. These considerations lead to the following hypothesis: Any motion of the defects entails a collective reorientation of *all* the spins. Indeed, the single particle diffusion constant D_i is at least an order of magnitude greater than D_d for all the system sizes and temperatures we studied. We point out that this type of motion is unlike the motion of point defects (dislocations) in crystals, which only requires a local rearrangement of particles to move the dislocation.

We try a rather crude test of this explanation. Let the single spin characteristic re-orientation time scale be set by $\tau_i = 1/D_i$, which is independent of system size (see Fig. 8). We then assume that the time scale for reorientation of all the spins on the sphere τ is approximately $\tau \sim N\tau_i$. With this assumption, we would expect that $1 \sim N D_\mathrm{d}/D_i$. We can (very approximately) collapse the points onto a single curve using

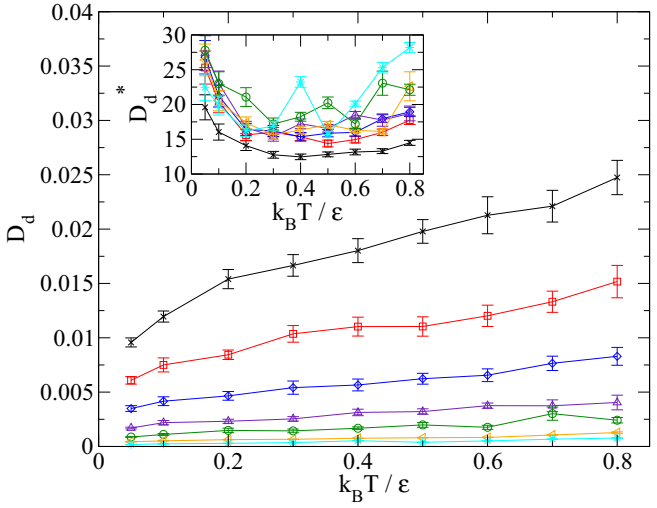

FIG. 12. (Color online) The defect diffusion constant D_d as a function of temperature for various system sizes extracted from fits to Eq. (23). (Inset) Same data with D_d scaled by system size; see main text. Lines are guides for the eye.

the scaling $D_\mathrm{d}^* = N D_\mathrm{d}/D_i$; see the inset in Fig. 12. Given the crudeness of our assumptions, it should not come as a surprise that D_d^* deviates from unity. However, the approximate data collapse is, in our view, a hint that the above reasoning can serve as a reasonable starting point for a more sophisticated analysis.

IV. CONCLUDING REMARKS

This work represents a study of defect motion and nematic ordering on a spherical surface using a variant of the Lebwohl-Lasher model. We find a very smooth transition from disordered to ordered phase upon decreasing the temperature and that the presence of defects raises the potential energy of the system compared to the planar case. The Frank elastic constant was determined for the various system sizes. They were found to vary considerably from the planar case, although they retain the $\sim S_{2i}^2$ dependence, as predicted by a simple mean-field approximation (Appendix C). The four $+1/2$ topological defects on the sphere surface exhibit subdiffusive behavior, with a diffusion constant orders of magnitude lower than the single spin diffusion constant.

Our strictly two-dimensional model could be extended with out-of-plane fluctuations of the orientation, which may be better suited to real systems of particle-stabilized droplets, where ellipsoid-shaped colloids have been shown to protrude into the surrounding solvent [29]. It would also be very interesting to see whether off-lattice liquid crystal models also exhibit similar behavior, in particular to see whether the defects move through a global or local rearrangement of the liquid crystal molecules. An analysis of the subdiffusive behavior of defect motion from a statistical mechanics of collective phenomena point of view would also be desirable.

ACKNOWLEDGMENTS

A.L. would like to acknowledge an interesting discussion with Aleksandr Donev about the defect dynamics and both A.L. and P.I. would like to thank Hans Christian Öttinger for critical comments on an earlier version of this paper.

APPENDIX A: MEAN-FIELD APPROXIMATION

The mean-field approximation to the Lebwohl-Lasher Hamiltonian H^MF is given by Eq. (2). From the Boltzmann distribution $\psi \sim e^{-\beta H^\mathrm{MF}}$, we identify the single particle potential and write the distribution function as

$$\psi(\phi) = \frac{1}{Z}\exp\left[2\alpha Q T_2(\cos\phi) - 2\alpha Q^2\right], \tag{A1}$$

with $\alpha = z\beta\varepsilon$, Z the partition function, and ϕ the angle between $\mathbf{u}_i$ and $\mathbf{n}$. From the relation $2Q = \langle T_2(\mathbf{u}\cdot\mathbf{n})\rangle$, where $\langle\cdots\rangle$ is an average over the distribution function (A1), we arrive at the self-consistency relation for the order parameter

$$Q = \frac{1}{2}\frac{\int_0^{2\pi} d\phi\, T_2(\cos\phi)\exp\left[2\alpha Q T_2(\cos\phi)\right]}{\int_0^{2\pi} d\phi\, \exp\left[2\alpha Q T_2(\cos\phi)\right]} = \frac{1}{2}\frac{I_1(2\alpha Q)}{I_0(2\alpha Q)}, \tag{A2}$$

where the terms $\exp(-2\alpha Q^2)$ have canceled. This expression was obtained earlier in Ref. [16]. Expanding Eq. (A2) in the limit $\alpha Q \to 0$, we obtain

$$Q \approx \tfrac{1}{2}\alpha Q - \tfrac{1}{4}(\alpha Q)^3 + \cdots, \tag{A3}$$

from which we find the mean-field prediction for the transition temperature:

$$k_B T_c^{MF}/\varepsilon = z/2. \tag{A4}$$

APPENDIX B: CALCULATION OF THE MEAN LOCAL ORDER PARAMETER IN THE ISOTROPIC STATE

The local order parameter S_{2i} is defined as two times the positive eigenvalue of $\mathbf{Q}_i$. In two dimensions, the orientation vector of a spin can be written $\mathbf{u}_j = (\cos\theta_j, \sin\theta_j)$, where $\theta_j \in [-\pi,\pi]$. Therefore, we write the local order parameter as

$$S_{2i} = 2\,\mathrm{eig}(\mathbf{Q}_i) = 2\left\{\frac{1}{N_i}\sum_{j=1}^{N_i}[(\cos^2\theta_j - 1/2)^2 + (\sin\theta_j\cos\theta_j)^2]\right\}^{1/2}, \tag{B1}$$

where N_i is the number of spins we average over to determine the local order parameter. The mean local order parameter is then Eq. (B1) averaged over the distributions of $\theta_1,\theta_2,\ldots,\theta_{N_i}$, which are all flat and normalized by $1/(2\pi)$ since we are in the isotropic phase. Taking this into account we calculate the integral

$$\langle S_{2i}\rangle = \frac{2}{(2\pi)^{N_i}}\int_{-\pi}^{\pi}\cdots\int_{-\pi}^{\pi}\left\{\frac{1}{N_i}\sum_{j=1}^{N_i}[(\cos^2\theta_j - 1/2)^2 + (\sin\theta_j\cos\theta_j)^2]\right\}^{1/2} d\theta_1\cdots d\theta_{N_i} \tag{B2}$$

$$= \frac{1}{\sqrt{N_i}}. \tag{B3}$$

APPENDIX C: CALCULATION OF ELASTIC CONSTANTS

In order to calculate the elastic constant K of the two-dimensional Lebwohl-Lasher model we adapt the argument of Priest [23,24] to the present case. Consider a distortion of the director field $\mathbf{n}(\mathbf{r})$. The orientation of rotor i is distributed around the local director $\mathbf{n}$ according to the distribution function $\psi(\mathbf{u}_i\cdot\mathbf{n})$. Starting from the Hamiltonian (1), $H = \frac{1}{2}\sum_{\langle i,j\rangle} v_{ij}$, we define the average interaction energy $\langle v_{ij}\rangle$ of two rotators,

$$\langle v_{12}\rangle(\mathbf{n},\mathbf{n}') = -\varepsilon\int d\theta_1\int d\theta_2\,\psi(\mathbf{n}\cdot\mathbf{u}_1)\psi(\mathbf{n}'\cdot\mathbf{u}_2)T_2(\mathbf{u}_1\cdot\mathbf{u}_2), \tag{C1}$$

where the integrals are over all possible orientations of the rotators. The single particle distribution function ψ can be expanded in Chebychev polynomials,

$$\psi(\mathbf{n}\cdot\mathbf{u}_1) = \sum_k \frac{c_k}{2\pi} S_k T_k(\mathbf{n}\cdot\mathbf{u}_1), \tag{C2}$$

where due to head-tail symmetry only even terms are included in the sum. The order parameters are defined by $S_k = \int_0^{2\pi} d\theta\, T_k(\cos\theta)\psi(\theta)$ with $c_k = 1$ for $k = 0$ and otherwise $c_k = 2$. With this expansion and the orthogonality of the Chebychev polynomials we arrive at $\langle v_{12}\rangle(\mathbf{n},\mathbf{n}') = -\varepsilon S_2^2 T_2(\mathbf{n}\cdot\mathbf{n}')$. Therefore, the free energy increase of the pair interaction due to director distortions is

$$\Delta\langle v_{12}\rangle = -\varepsilon S_2^2[T_2(\mathbf{n}\cdot\mathbf{n}') - 1] = 2\varepsilon S_2^2\sin^2\alpha, \tag{C3}$$

where α is the angle formed by the director field at two neighboring lattice sites. The local free-energy density increase at lattice point i follows from $\Delta f(\mathbf{r}_i) = \frac{1}{2}\sum_{\langle i,j\rangle}\Delta\langle v_{ij}\rangle$, where the sum runs over nearest neighbors of site i.

Specializing to a square lattice with lattice constant a, let the distortion field be represented by the Fourier series with wave vector $\mathbf{q}$ oriented parallel to the x axis. Then the free-energy density increase becomes

$$\Delta f = \frac{2\varepsilon S_2^2}{a^2}\sin^2(qa). \tag{C4}$$

For small wave vectors, we recover from Eq. (C4) the continuum limit $\Delta f = \frac{1}{2}Kq^2$ and read off the value of the Frank elastic constant $K_{sq} = 4\varepsilon S_2^2$. Repeating the argument for the triangular lattice with lattice vectors $\mathbf{a}_1 = a\hat{\mathbf{x}}$ and $\mathbf{a}_2 = a(\hat{\mathbf{x}} + \sqrt{3}\hat{\mathbf{y}})/2$, we arrive at the corresponding result $K_{hex} = 6\varepsilon S_2^2$.

APPENDIX D: ALTERNATIVE ROUTE TO EXTRACTING THE FRANK ELASTIC CONSTANT FROM SIMULATION DATA

The free energy F_d in terms of the angle β_{ij} between different defects i and j on a nematic spherical shell is given by [3]

$$F_d = \frac{\pi K_s}{8}\sum_{i\neq j} n_i n_j \ln(1-\cos\beta_{ij}) + E\sum_j n_j^2, \tag{D1}$$

where n_i is the topological charge of defect i and E is the phenomenologically added defect self-energy, which is difficult to determine. From the simulation data we can obtain a time series of the potential energy and of the angles β_{ij}. Since the defect self-energy should be constant in time, we can extract an estimate for the elastic constant using

$$\mathrm{Var}(F_d) = \left(\frac{\pi K}{32}\right)^2 \mathrm{Var}\left[\sum_{i\neq j}\ln(1-\cos\beta_{ij})\right], \tag{D2}$$

where $\mathrm{Var}(\cdots)$ denotes the variance of the quantity in brackets and $n_i = 1/2$. Using the variance eliminates any constant contributions to the free energy such as the defect self-energy. However, since the variance in free energy contains a contribution from thermal fluctuations, this method leads to an overestimate of K_s. To help remedy this, one can extrapolate K_s to zero T to remove the effect of thermal fluctuations.

[1] T. C. Lubensky, Solid State Commun. **102**, 187 (1997).
[2] G. Crawford and S. Zumer, *Liquid Crystals in Confined Geometries* (Taylor & Francis, London, 1996).
[3] M. J. Bowick and L. Giomi, Adv. Phys. **58**, 449 (2009).
[4] D. R. Nelson, Nano Lett. **2**, 1125 (2002).
[5] T. C. Lubensky and J. Prost, J. Phys. II **2**, 371 (1992).
[6] A. Fernandez-Nieves, V. Vitelli, A. S. Utada, D. R. Link, M. Marquez, D. R. Nelson, and D. A. Weitz, Phys. Rev. Lett. **99**, 157801 (2007).
[7] H. Shin, M. J. Bowick, and X. Xing, Phys. Rev. Lett. **101**, 037802 (2008).
[8] T. Lopez-Leon, V. Koning, K. B. S. Devaiah, V. Vitelli, and A. Fernandez-Nieves, Nat. Phys. **7**, 391 (2011).
[9] D. Šec, T. Lopez-Leon, M. Nobili, C. Blanc, A. Fernandez-Nieves, M. Ravnik, and S. Žumer, Phys. Rev. E **86**, 020705 (2012).
[10] G. Skačej and C. Zannoni, Phys. Rev. Lett. **100**, 197802 (2008).
[11] V. Vitelli and D. R. Nelson, Phys. Rev. E **74**, 021711 (2006).
[12] G. Lasher, J. Comp. Phys. **53**, 4141 (1970).
[13] P. A. Lebwohl and G. Lasher, Phys. Rev. A **6**, 426 (1972).
[14] Z. Zhang, O. G. Mouritsen, and M. J. Zuckermann, Phys. Rev. Lett. **69**, 2803 (1992).
[15] E. Mondal and S. K. Roy, Phys. Lett. A **312**, 397 (2003).
[16] J. Y. Denham, G. R. Luckhurst, C. Zannoni, and J. W. Lewis, Mol. Cryst. Liq. Cryst. **60**, 185 (1980).
[17] S. E. Bedford, T. M. Nicholson, and A. H. Windle, Liq. Cryst. **10**, 63 (1991).
[18] J. Ding and Y. Yang, Rheol. Acta **33**, 405 (1994).
[19] P. Palffy-Muhoray, Am. J. Phys. **70**, 433 (2002).
[20] A. M. Luo, L. M. C. Sagis, and P. Ilg, J. Chem. Phys. **140**, 124901 (2014).
[21] P. Ilg, Phys. Rev. E **85**, 061709 (2012).
[22] P. G. de Gennes and J. Prost, *The Physics of Liquid Crystals*, 2nd ed. (Clarendon Press, Oxford, UK, 1993).
[23] D. J. Cleaver and M. P. Allen, Phys. Rev. A **43**, 1918 (1991).
[24] R. G. Priest, Mol. Cryst. Liq. Cryst. **17**, 129 (1972).
[25] Y. Kurihara and L. Holloway, Mon. Weather Rev. **95**, 509 (1967).
[26] E. S. Popko, *Divided Spheres: Geodesics and the Orderly Subdivision of the Sphere* (CRC Press, Boca Raton, FL, 2012).
[27] D. H. Van Winkle and N. A. Clark, Phys. Rev. A **38**, 1573 (1988).
[28] A. Feder, Y. Tabe, and E. Mazur, Phys. Rev. Lett. **79**, 1682 (1997).
[29] B. Madivala, S. Vandebril, J. Fransaer, and J. Vermant, Soft Matter **5**, 1717 (2009).